Journal of Marine Science and Application (2019) 18:325–333
https://doi.org/10.1007/s11804-019-00079-5

RESEARCH ARTICLE

# Array Characteristics of Oscillating-Buoy Two-Floating-Body Wave-Energy Converter

Renwei Ji[1,2] · Qihu Sheng[1,2] · Shuqi Wang[3] · Yuquan Zhang[4] · Xuewei Zhang[1,2] · Liang Zhang[1,2]

Received: 26 July 2018 / Accepted: 18 November 2018 / Published online: 1 April 2019


## Abstract

As the energy supply problem worsens, the development and utilization of marine renewable energy have become a research hotspot. The development of wave energy is moving from the near shore to the distant sea. The power-generation efficiency of a single two-floating-body wave-energy converter is relatively low. To fully utilize wave energy and improve the wave-energy capture rate of a fixed sea area, arranging a two-floating-body wave-energy converter array is necessary. This paper first introduces the basic theory of multi-floating flow field, time-domain calculation method, and influence factor of the wave-energy converter array. Then, the development of AQWA software in Fortran language considers the effect of power takeoff. A calculation method based on ANSYS–AQWA is proposed to simulate the motion of the oscillating-buoy two-floating-body wave-energy converter. The results are compared with the experimental results from the National Renewable Energy Laboratory. Finally, the ANSYS–AQWA method is used to study the power characteristics of simple and complex arrays of wave-energy converters. The average power generation of simple arrays is largest at 0°, and the average power generation of complex arrays does not change with the wave direction. Optimal layout spacing exists for the simple and complex arrays. These findings can serve as a valuable reference for the large-scale array layout of wave-energy converters in the future.

**Keywords** Oscillating buoy · Two-floating body · Wave-energy converter · AQWA · Converter array · Power characteristics

## 1 Introduction

With the rapid development of the global economy, the demand for and dependence of countries on energy is increasing (Gunn and Stock-Williams 2012). Fossil energy still accounts for a large proportion of the overall energy structure. According to the current speed of development of the mining industry, we are likely to face a serious energy crisis and environmental pollution in China (Guan 2011; Zhao et al. 2008). Thus, developing and using renewable energy are imperative (Xu et al. 2018). As an important part of marine renewable energy, wave energy has advantages of large reserves, cleanliness, and broad development prospects. As an important structure for the development of wave energy, the oscillating-buoy wave-energy converter has become a research hotspot in China and abroad due to its simple structure, high energy-conversion efficiency, and wide-frequency response range (Li and He 2013). The development of wave energy is moving from the near shore to the distant sea. However, the power generation efficiency of a single two-floating-body wave-energy converter is relatively low and cannot meet the requirements. To fully utilize wave energy

**Article Highlights**
- As the energy problem worsens, the array layout of the two-floating-body wave-energy converter becomes an inevitable trend.
- The influence of power takeoff is considered through Fortran's secondary development.
- Two different array layouts (simple and complex) are proposed, and corresponding conclusions are drawn. The layout of complex arrays provides insights into the design of subsequent multi-energy complementary energy-island platforms.

✉ Qihu Sheng
shengqihu@hrbeu.edu.cn

[1] College of Shipbuilding Engineering, Harbin Engineering University, Harbin 150001, China

[2] Institute of Ocean Renewable Energy System, Harbin Engineering University, Harbin 150001, China

[3] College of Naval Architecture and Ocean Engineering, Jiangsu University of Science and Technology, Zhenjiang 212001, China

[4] College of Energy and Electrical Engineering, Hohai University, Nanjing 211100, China

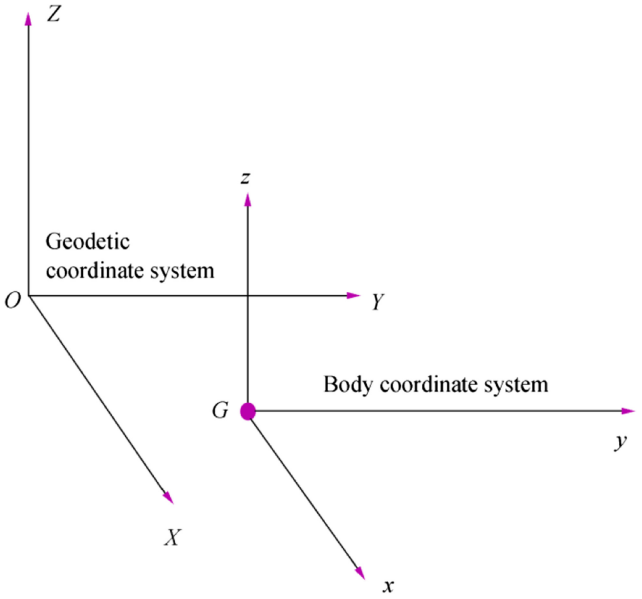


**Fig. 1** Coordinate system

and improve the wave-energy capture rate of fixed sea areas, scholars have been studying how to arrange two-floating-body wave-energy converters in a fixed sea area (Dai 2015).

Thomas and Evans (1981) examined the characteristics of wave-energy converters in waves and the mutual interference between floating bodies in waves. Eriksson et al. (2005) studied the hydrodynamic characteristics of a bottom-contacting cylindrical wave-energy converter under linear power takeoff (PTO). Garnaud and Mei (2009) used the densely arranged oscillating-buoy wave-energy converter array as the research object and proposed the calculation formula of hydrodynamic influence. Child and Venugopal (2010) and Child (2011) proposed genetic algorithms and parabolic cross-section methods to optimize arrays of wave-energy converter. Borgarino et al. (2012) conducted a series of studies on the array layout of single-floating-body wave-energy converters and found that the array layout of triangles is relatively optimal. Wolgamot et al. (2012) found that the wave direction has a greater impact on the power of the wave-energy converter array. Nazari et al. (2013) found that the natural frequency and damping coefficient of the oscillating floating body significantly affect the vertical displacement of the floating body. Guo et al. (2018) studied the hydrodynamic performance of wave-energy converters under nonlinear PTO.

Thus far, domestic and foreign scholars have focused on single-floating-body wave-energy converters, which involve hydrodynamic performance, motion characteristics, power features, and control methods. Few studies have been conducted on two-floating-body wave-energy converters and their arrays. Therefore, this paper proposes an ANSYS–AQWA method based on the potential flow theory to study the power characteristics of the oscillating-buoy two-floating-body wave-energy converter array. The details are as follows:

1) The basic theory (including the basic theory of multi-floating flow field and time-domain calculation method of floating body) is introduced.
2) Based on the potential flow theory, a method of ANSYS–AQWA is proposed, and the development of AQWA software is included in the PTO influence through the Fortran language. The motion simulation of the oscillating-buoy two-floating-body wave-energy converter is achieved, and the results of the calculation are compared with the experiment of the National Renewable Energy Laboratory (NREL) of the United States.
3) Introducing the influence factor of the wave-energy converter array, the ANSYS–AQWA calculation method is used to study the influence of the arrangement spacing and wave direction on the power characteristics of the wave-energy converter in simple and complex arrays.

## 2 Basic Theory and Method

### 2.1 Floating-Body Moving Coordinate System

As shown in Fig. 1, the coordinate system includes the geodetic coordinate and body coordinate systems. The origin of the geodetic coordinate system is located on the hydrostatic surface, the *Z*-axis is perpendicular to the hydrostatic surface (Chen 2013), and the origin of the body coordinate system is located at the center of gravity of the floating body. In the initial case, the respective coordinate axes of the body coordinate system are parallel to the axes of the geodetic coordinate system. The movement of the floating body can be reflected

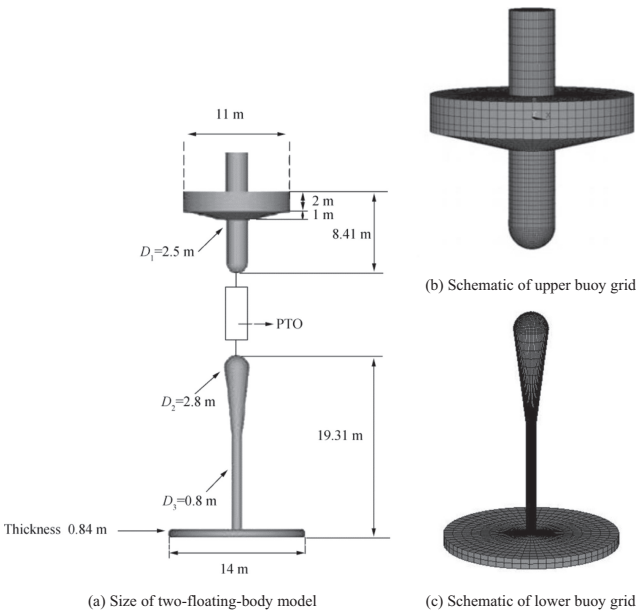


**Fig. 2** Two-floating-body model and grid schematic

**Table 1** Related parameters of upper and lower buoys

| Buoy | Weight/kg | Center of gravity/m | Draft/m |
|---|---|---|---|
| Upper buoy | 8.45E+04 | (0, 0, − 0.4) | 1.63 |
| Lower buoy | 1.65E+05 | (0, 0, − 28.4) | 34.97 |

by the position of the body coordinate system *Gxyz* in the geodetic coordinate system *OXYZ*.

## 2.2 Basic Theory of Multi-floating-body Flow Field

### 2.2.1 Velocity Potential of Multi-floating-body Flow Field

When multiple floating bodies exist in the flow field, these bodies affect one another. The velocity potential $\Phi$ of the multi-floating flow field can be divided into incident wave potential $\Phi_{\mathrm{I}}$, diffraction potential $\Phi_{\mathrm{D}}$, and radiation potential $\Phi_{\mathrm{R}}$. The multiple floating bodies move in the flow field, and the radiation potential of each floating body includes the superposition of its own radiation potential and the radiation potential of other floating bodies.

Based on the assumption that $N$ floating bodies exist in a flow field, the total velocity potential of the flow field is:

$$\Phi = \Phi_{\mathrm{I}} + \Phi_{\mathrm{D}} + \sum_{m=1}^{N} \Phi_{\mathrm{R}}^{(m)} \tag{1}$$

where $\Phi_{\mathrm{R}}^{(m)}$ is the radiation potential generated by the $m$-th floating body.The radiation potential $\Phi_{\mathrm{R}}^{(m)}$ of the $m$-th floating body in the multi-floating body is

$$\Phi_{\mathrm{R}}^{(m)}(x,y,z,t) = \mathrm{Re}\left(\phi_{\mathrm{R}}^{(m)}(x,y,z)e^{-\mathrm{i}\omega t}\right) \tag{2}$$

$$\phi_{\mathrm{R}}^{(m)}(x,y,z) = -\mathrm{i}\omega \bar{z}_j^{(m)} \phi_j^{(m)} \ (j = 1,2,\cdots,6) \tag{3}$$

where $\bar{z}_j^{(m)}$ is the amplitude of the $m$-th floating body as the plural movement of the $j$-state, and $\phi_j^{(m)}$ is the velocity potential of the $m$-th floating body moving only in the $j$-state at the unit speed.

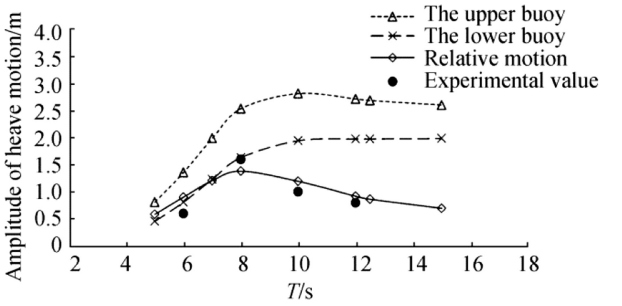


**Fig. 3** Comparison between numerical simulation result and experimental value

### 2.2.2 Hydrodynamic Coefficient of Multi-floating-body Flow Field

Based on the linearized Bernoulli equation, the dynamic pressure of floating body can be obtained:

$$p = -\rho \frac{\partial \Phi}{\partial t} \tag{4}$$

When the floating body $B_a$ is moving, the $j$-state component $F_j^{(m,a)}$ of the floating body $B_m$ is

$$F_j^{(m,a)} = \iint_{S_m} p\tilde{n}_j^{(m)} \mathrm{d}s = \mathrm{Re}\left\{ \rho\omega^2 \bar{z}_k^{(a)} \mathrm{e}^{-\mathrm{i}\omega t} \iint_{S_m} \phi_k^{(a)} \tilde{n}_j^{(m)} \mathrm{d}s \right\} \tag{5}$$

Analogous to the derivation of hydrodynamic coefficients of single-floating body, the radiation surface condition $\frac{\partial \phi_j^{(m)}}{\partial n^i} = \tilde{n}_j^{(m)}$ is substituted into Eq. (5), and Eq. (6) is introduced. Subsequently, Eq. (7) can be derived from the previous equations:

$$\lambda_{jk}^{(m,a)} + \mathrm{i}\frac{\mu_{jk}^{(m,a)}}{\omega} = \rho \iint_{S_m} \phi_k^{(a)} \frac{\partial \phi_j^{(m)}}{\partial n_j^{(m)}} \mathrm{d}s \tag{6}$$

$$\begin{aligned} F_j^{(m,a)} &= \mathrm{Re}\left\{ \mathrm{e}^{-\mathrm{i}\omega t} \omega^2 \bar{z}_k^{(a)} \left( \lambda_{jk}^{(m,a)} + \mathrm{i}\frac{\mu_{jk}^{(m,a)}}{\omega} \right) \right\} \\ &= -\ddot{z}_k^{(a)} \lambda_{jk}^{(m,a)} - \dot{z}_k^{(a)} \mu_{jk}^{(m,a)} \end{aligned} \tag{7}$$

Among them, $j = 1, 2, \cdots, 6$ is the free index, $k = 1, 2, \cdots, 6$ is the dummy index, $\lambda_{jk}^{(m,a)}$ is the additional mass coefficient

**Table 2** Numerical simulation results of two-floating-body wave-energy converter

| Wave period/s | 5 | 6 | 7 | 8 | 10 | 12.0 | 12.5 | 15 |
|---|---|---|---|---|---|---|---|---|
| Motion amplitude of upper buoy/m | 0.81 | 1.36 | 1.99 | 2.54 | 2.82 | 2.72 | 2.69 | 2.61 |
| Motion amplitude of lower buoy/m | 0.46 | 0.81 | 1.23 | 1.64 | 1.95 | 1.98 | 1.98 | 1.99 |
| Relative motion amplitude/m | 0.59 | 0.91 | 1.21 | 1.38 | 1.20 | 0.92 | 0.86 | 0.70 |
| Experimental value/m | – | 0.6 | – | 1.6 | 1 | 0.8 | – | – |

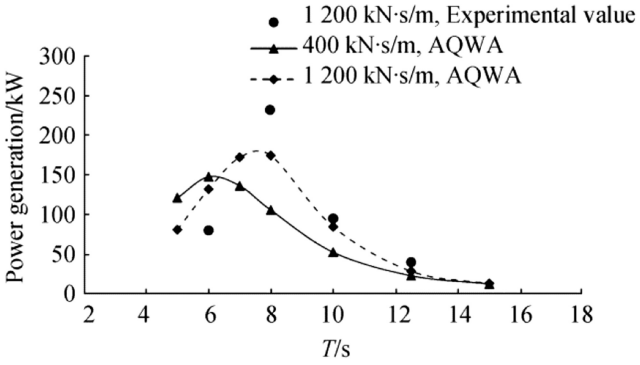


**Fig. 4** Power characteristics under different PTO damping coefficients

of the multi-floating body, and $\mu_{jk}^{(m,a)}$ is the damping coefficient of the multi-floating body.

According to Green's second formula, the symmetry between $\mu_{jk}^{(m,a)}$ and $\mu_{kj}^{(a,m)}$, $\lambda_{jk}^{(m,a)}$ and $\lambda_{kj}^{(a,m)}$ can be obtained.

To sum up, the force of the $m$-th floating body is

$$F_j^{(m)} = \sum_{a=1}^{N} -\ddot{z}_k^{(a)} \lambda_{jk}^{(m,a)} - \dot{z}_k^{(a)} \mu_{jk}^{(m,a)} \tag{8}$$

## 2.3 Time-Domain Calculation Method of Floating Body

### 2.3.1 Time-Domain Equation of Motion

In actual engineering, the force and displacement of the floating body are nonlinear, so the time-domain calculation method is adopted. The time-domain calculation method of the floating body is classified into direct and indirect methods.

The direct method aims to calculate the motion equation of the floating body by solving the Green function in the time domain. This method requires re-division of the mesh of the structural wet surface at all times during the calculation, thereby consuming a large amount of time and computational resources.

The indirect method (calculation method used by AQWA) is derived from the impulse response method, which considers the motion of the floating body as a superposition of a series of pulse motions. Therefore, the force received by the floating body can be regarded as a superposition of a series of linear forces, which establishes a relationship between force and motion. Thus, the equation of motion of the floating body is established, as shown in Eq. (9). The frequency domain results are transformed into time-domain hydrodynamic parameters in the motion equation by fast Fourier transform. This indirect time-domain method is simple to calculate and widely used:

$$(\boldsymbol{M} + \boldsymbol{\lambda})\ddot{z}(t) + \int_{-\infty}^{t} \boldsymbol{K}(t-\tau)\dot{z}(t)\mathrm{d}\tau + \boldsymbol{C}x(t) = \boldsymbol{F}(t) \tag{9}$$

where $\boldsymbol{M}$ is the generalized mass matrix of the floating body, $\boldsymbol{\lambda}$ is the additional mass matrix, $\boldsymbol{K}(t-\tau)$ is the delay function of the system, $\boldsymbol{C}$ is the hydrostatic recovery stiffness of the floating-body structure, and $\boldsymbol{F}(t)$ is the generalized force matrix received by the floating body.

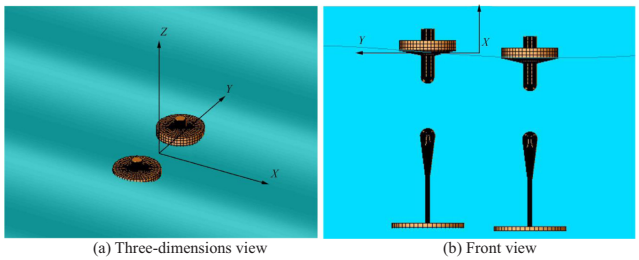


(a) Three-dimensions view (b) Front view

**Fig. 5** Schematic of two-floating-body wave-energy converter array

### 2.3.2 Time-Domain Motion Equation of Array

We assume the existence of an $m \times n$ array consisting of the same floating. The floating in the array is not only subject to the wave forces generated by the wave incidence but also by the wave forces generated by the diffraction and radiation effects of the various floating in the array. According to the literature (Sinha et al. 2016), the time-domain motion equations of each floating can be obtained:

$$\begin{aligned}&(M_{ij} + \lambda_{ij})\ddot{z}_{ij}(t) + \mu_{ij}\dot{z}_{ij}(t) + (C_{ij} + c_{ij})z_{ij}(t) + \\ &\int_0^t K_{ij}(t-\tau)\dot{z}_{ij}(\tau)\mathrm{d}\tau = F_{ij}(t) + \sum_{i=1}^{n}\sum_{j=1}^{m} f_{i,j}(h_{i,j}, t)\end{aligned} \tag{10}$$

Among them, $\ddot{z}_{ij}(t)$, $\dot{z}_{ij}(t)$, and $z_{ij}(t)$ are the acceleration, velocity, and displacement of the floating, respectively; $M_{ij}$ is a generalized mass matrix; $C_{ij}$ is the restoring force coefficient matrix; and $\lambda_{ij}$, $\mu_{ij}$, and $c_{ij}$ are instantaneous response terms, which are related to the additional mass, damping coefficient, and restoring force coefficient, respectively. $K_{ij}(t)$ is the delay function related to the shape of the floating and time interval. $F_{ij}(t)$ is the wave force acting on the floating at time $t$. $h_{i,j}$ is the spacing between the $i$-th and $j$-th floating. $\sum_{i=1}^{n}\sum_{j=1}^{m} f_{i,j}(h_{i,j}, t)$ is the sum of the diffraction wave forces acting on a floating at time $t$ (Zhang and Dai 1992).

### 2.3.3 Time-Domain Analysis Method Based on Potential Flow Theory

Based on the potential flow theory, a time-domain analysis method for studying the characteristics of the two-floating-body wave-energy converter is proposed by combining Fortran with ANSYS–AQWA software. The main issues in studying the characteristics of two-floating-body wave-energy

**Table 3** Simulation parameters under different arrangement spacing

| Wave period/s | Wave height/ m | Wave direction/ (°) | PTO stiffness coefficient/ ($kN{\cdot}m^{-1}$) | PTO damping coefficient/ ($kN{\cdot}s{\cdot}m^{-1}$) | Arrangement spacing/m |
|---|---|---|---|---|---|
| 8 | 2.5 | 0 | 20 | 1200 | 15–80 |

**Table 4** Average power generation of wave-energy array with different spacing

| Arrangement spacing/m | 15 | 20 | 25 | 30 | 35 | 40 | 45 | 50 | 60 | 70 | 80 |
|---|---|---|---|---|---|---|---|---|---|---|---|
| Power/kW | 178.7 | 190.9 | 199.3 | 204.3 | 205.9 | 204.3 | 200.2 | 194.6 | 182.9 | 175.0 | 173.0 |

converters by time-domain analysis are (1) hydrodynamic interference between the upper and lower buoys, (2) influence of the heave damping plate (Teng et al. 2010), and (3) influence of the PTO device between the upper and lower buoys.

### 2.4 Influence Factors of Wave-Energy Converter Array

The wave-energy array influence factor $q$ is an important indicator for measuring the power characteristics of wave-energy converter array (Zhang 2015). Based on the assumption that the wave-energy array is composed of $N$ identical wave-energy converters, the wave-energy array influence factor $q$ can be expressed as:

$$q = \frac{P_{\text{arrays}}}{N \cdot P} \tag{11}$$

where $P_{\text{arrays}}$ is the total power generation of the wave-energy array composed of $N$ two-floating-body wave-energy converters, and $P$ is the power generation of a single two-floating-body wave-energy converter. If $q > 1$, then the hydrodynamic interference between the wave-energy arrays is beneficial; if $q < 1$, then the interference between the wave-energy arrays is detrimental. Studies by Budal (1977), Evans (1979), and Falnes (1980) have shown that the influence factor $q$ may be larger than 1 or smaller than 1 depending on the frequency of the incident wave and arrangement of the two-floating-body wave-energy array. This finding shows that by adjusting the array layout of the two-floating-body wave-energy converter, the total power generation of the wave-energy array can become larger than the sum of the power of the single two-floating-body wave-energy converter.

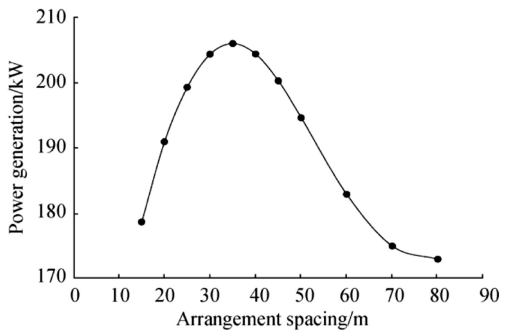


**Fig. 6** Variation of average power generation of wave-energy array with arrangement spacing

## 3 Numerical Verification

### 3.1 Establishment of Model

The model of the two-floating-body wave-energy converter is composed of the upper and lower buoys, as shown in Fig. 2. The related parameters are presented in Table 1.

### 3.2 Feasibility Verification

This study only considers the heave motion of the upper and lower buoys. To verify the feasibility of calculating the two-floating-body wave-energy converter by ANSYS–AQWA, the regular wave is selected, the wave height is 2.5 m, the wave period is different, and the PTO is simulated by the mass-spring-damping system. The stiffness of the spring is 20 kN/m, and the damping is 1200 kN·s/m. The total time taken in numerical simulation is 500 s and the time step 0.5 s.

The results of the numerical simulation are shown in Table 2 and compared with the results in the literature (Yu and Li 2013). Thus, Fig. 3 can be obtained.

Figure 3 shows that the amplitude of the relative motion between the upper and lower buoys obtained by numerical simulation is in good agreement with the experimental value. The amplitude of the upper buoy heave motion is at maximum when the wave period is 10 s. No peak is observed in the lower buoy movement process. The heave motion increases with the increase of the wave period. The amplitude of relative motion

**Table 5** Simulation parameters under different wave directions

| Wave period/s | Wave height/m | Wave direction/(°) | PTO stiffness coefficient/ ($kN \cdot m^{-1}$) | PTO damping coefficient/ ($kN \cdot s \cdot m^{-1}$) | Arrangement spacing/m |
|---|---|---|---|---|---|
| 8 | 2.5 | 0, 30, 60, 90 | 20 | 1200 | 15–80 |

between the upper and lower buoys reaches the maximum value at the wave period of 8 s.

Power generation is an important indicator in evaluating a wave-energy converter. The average power of the two-floating-body wave-energy converter is determined by selecting the average value of the instantaneous power of the last five wave periods. The instantaneous power can be determined according to the time history curve of the velocity of the upper and lower buoys. The calculation results are presented in Fig. 4.

Figure 4 describes the power variation of a two-floating-body wave-energy converter with the wave period under different PTO damping coefficients. The following conclusions are drawn:

1) When the damping coefficient is 1200 kN·s/m, the results of the AQWA simulation agree well with the experimental results, except for the resonance period because of errors in the experimental and numerical models.
2) Different PTO damping coefficients correspond to different rates of optimal absorption power.

## 4 Results and Analysis

In an array of two-floating-body wave-energy converters, the mutual hydrodynamic interference between the wave-energy converters ultimately affects the wave-energy capture rate of the array. Considering the ever-changing arrangement of the wave-energy converter, a simple array of two wave-energy converters and a complex array of six wave-energy converters are selected as research objects. The power characteristics of the two-floating-body wave-energy converter array are studied by using the time-domain method.

**Table 6** Average power generation of wave-energy array with different wave directions

| Wave direction/ (°) | Spacing/m | | | | | | |
|---|---|---|---|---|---|---|---|
| | 15 | 20 | 25 | 30 | 35 | 40 | 45 |
| 0 | 178.7 | 190.9 | 199.3 | 204.3 | 205.9 | 204.4 | 200.2 |
| 30 | 180.0 | 189.3 | 193.3 | 193.6 | 191.5 | 188.3 | 185.4 |
| 60 | 182.4 | 186.2 | 183.7 | 178.5 | 173.6 | 171.2 | 171.8 |
| 90 | 183.4 | 184.9 | 179.9 | 173.4 | 168.8 | 167.8 | 165.0 |

### 4.1 Simple Array

A simple array consisting of two identical two-floating-body wave-energy converters is shown in Figure 5. The influence of wave direction and arrangement spacing on the power characteristics of the wave-energy converter array is studied by using the time-domain method.

#### 4.1.1 Influence of Arrangement Spacing on Power Characteristics of Array

The arrangement spacing of the two-floating-body wave-energy converter is the main parameter that affects the power generation of the array. This section examines the influence of the arrangement spacing on the power generation. The simulation parameters are shown in Table 3. The simulation results are reported in Table 4 and Fig. 6.

Figure 6 shows the variation of the average power generation of the single-wave-energy converter in the wave-energy array with the arrangement spacing when the wave period is 8 s and the wave direction is 0°. The figure shows that the average generating power of a single-wave-energy converter increases first and then decreases with the increase of the arrangement spacing, that is, an optimal arrangement spacing exists, which enables the power of the wave-energy converter array to reach the maximum. The maximum of the average

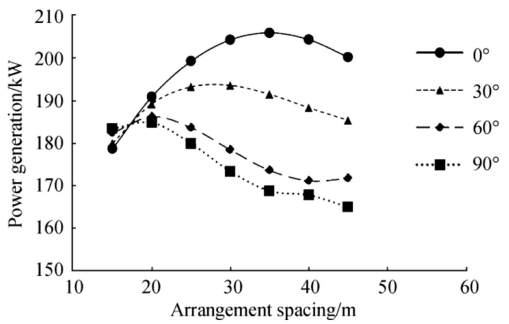


**Fig. 7** Variation of average power generation with wave direction for wave-energy array

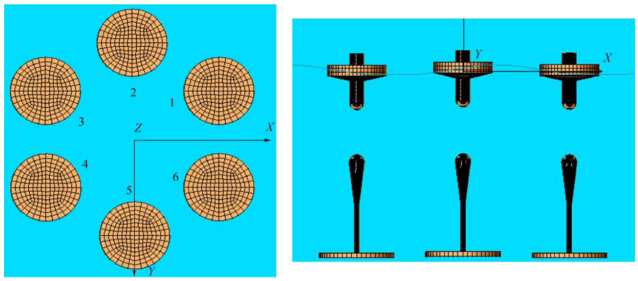


(a) Six-angle array arrangement (b) Six-angle array grid schematic

**Fig. 8** Complex (six-angle) array

array with the arrangement spacing under different wave directions. As shown in the diagram, the average power generation of a single-wave-energy converter increases first and then decreases with the increase of the spacing of the arrangement. An optimal arrangement spacing is observed. When the wave-energy converter is arranged perpendicular to the wave direction, the average power generation of a single-wave-energy converter is the largest. When the wave-energy converter is arranged along the wave direction, the average power generation of a single-wave-energy converter is at minimum.

**Table 7** Simulation parameters under different arrangement spacing

| Wave period/s | Wave height/m | Wave direction/(°) | PTO stiffness coefficient/ ($kN \cdot m^{-1}$) | PTO damping coefficient/ ($kN \cdot s \cdot m^{-1}$) | Arrangement spacing/m | Arrangement |
|---|---|---|---|---|---|---|
| 8 | 2.5 | 0 | 20 | 1200 | 20–80 | Six-angle array |

generating power is 12% higher than that of a single two-floating-body wave-energy converter. When the spacing is 30–40 m, the average generating power is the largest. With the increase of spacing, the area occupied by the sea increases, and the power generation is reduced. This condition should be avoided in engineering practice.

#### 4.1.2 Influence of Wave Direction on Power Characteristics of Array

If the layout of the wave-energy converter array is fixed, the different wave directions also affect the power generation of the wave-energy array. This section studies the effect of different wave directions on the wave-energy array. The specific simulation parameters are presented in Table 5, and the simulation results are shown in Table 6 and Fig. 7.

Figure 7 shows the variation of the average power generation of a single-wave-energy converter in the wave-energy

### 4.2 Complex Array

Based on the simple array, a complex (six-angle) array is proposed. The influence of arrangement spacing and wave direction on the power generation characteristics of the six-angle array is studied. As presented in Fig. 8, in the six-angle array, six wave-energy converters are surrounded by a circle with a radius of 20 m, and each two wave-energy converters form a 60° angle around the center of the circle.

#### 4.2.1 Influence of Arrangement Spacing on Power Characteristics of Array

The six-angle array is used as the research object to explore the effect of arrangement spacing on the average power characteristics of the array. The simulation parameters are shown in Table 7, and the simulation results are presented in Table 8.

**Table 8** Power generation of wave-energy converter with different arrangement spacing

| Arrangement spacing/m | WEC1 | WEC2 | WEC3 | WEC4 | WEC5 | WEC6 | Average power |
|---|---|---|---|---|---|---|---|
| 20 | 108.8 | 171.0 | 198.1 | 198.1 | 171.0 | 108.8 | 159.2 |
| 30 | 127.7 | 195.3 | 189.9 | 189.9 | 195.3 | 127.7 | 171.0 |
| 40 | 152.8 | 169.5 | 197.3 | 197.3 | 169.5 | 152.8 | 173.2 |
| 50 | 169.9 | 158.2 | 200.7 | 200.7 | 158.2 | 169.9 | 176.3 |
| 60 | 177.7 | 188.1 | 195.7 | 195.7 | 188.1 | 177.7 | 187.2 |
| 70 | 177.2 | 174.9 | 189.4 | 189.4 | 174.9 | 177.2 | 180.5 |
| 80 | 163.0 | 189.3 | 189.1 | 189.1 | 189.3 | 163.0 | 180.4 |

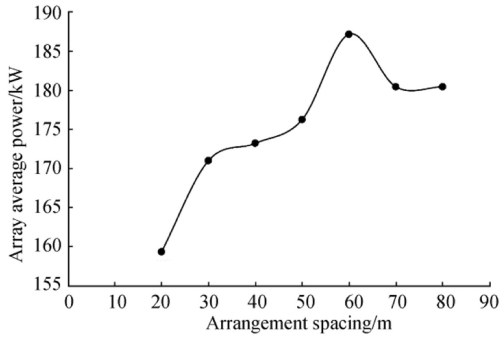


**Fig. 9** Average power generation of six-angle array under different arrangement spacing

The average power generation of the wave-energy converter array under different arrangement spacing in Table 8 is drawn in Fig. 9.

Figure 9 depicts the influence of different arrangement spacing on the average power generation of the six-angle array. The figure shows that with the increase of arrangement spacing in the six-angle array, the average power generation of the array first increases, then decreases, and then tends to be stable. An optimal arrangement spacing is observed due to the hydrodynamic interference between the wave-energy converters. With the increase of spacing, beneficial interference occurs, thereby causing an increase in the motion response of the wave-energy converter and the average power generation of the array. When the spacing increases to a certain extent, the interference between the wave-energy converters becomes extremely small and the average power generation of the array tends to be stable.

#### 4.2.2 Influence of Wave Direction on Power Characteristics of Array

Different wave directions affect the movement of the two-floating-body wave-energy converter, and further affect the power generation of the six-angle array. This section studies the effect of different wave directions on the power generation of the six-angle array. The specific simulation parameters are shown in Table 9, and the simulation results are reported in Table 10.

The average power generation of the wave-energy array under different wave directions in Table 10 is drawn in Fig. 10.

Figure 10 shows the variation of the average power generation of the six-angle wave-energy converter array with the wave direction. The average power of the six-angle array is almost invariable with the wave direction, and the absorption of wave energy is not affected by the direction of the coming flow, which is beneficial to the absorption of wave energy in the different wave directions in the real ocean environment. The design of the six-angle array is in accordance with engineering practice and provides new insights into the array layout of the wave-energy converter in the future.

## 5 Conclusions

This paper first introduced the basic theory of the two-floating-body wave-energy converter array and the calculation method in the time domain. Then, the motion model of the oscillating-buoy two-floating-body wave-energy converter was established, and the time-domain analysis method of ANSYS–AQWA based on the potential flow theory was proposed. This method was used to verify the two-floating-body wave-energy converters of NREL. The numerical results were consistent with the experimental values, and the accuracy and feasibility of the method were verified. Finally, a simple array and a complex array were selected as the research objects. The power characteristics of the two-floating-body wave-energy converter array were studied through the time-domain analysis method of ANSYS–AQWA. The research results are as follows:

**Table 9** Simulation parameters under different wave directions

| Wave period/s | Wave height/m | Wave direction/(°) | PTO stiffness coefficient/(kN·m$^{-1}$) | PTO damping coefficient/(kN·s·m$^{-1}$) | Arrangement |
|---|---|---|---|---|---|
| 8 | 2.5 | 0, 30, 60, 90 | 20 | 1200 | Six-angle array |

**Table 10** Power generation of wave-energy converter with different wave directions

| Wave direction/(°) | WEC1 | WEC2 | WEC3 | WEC4 | WEC5 | WEC6 | Average power |
|---|---|---|---|---|---|---|---|
| 0 | 108.8 | 171.0 | 198.1 | 198.1 | 171.0 | 108.8 | 159.2 |
| 30 | 103.3 | 134.2 | 191.9 | 198.9 | 192.7 | 134.9 | 159.3 |
| 60 | 109.6 | 109.1 | 170.8 | 198.6 | 198.8 | 171.9 | 159.8 |
| 90 | 135.2 | 103.6 | 135.2 | 193.1 | 199.5 | 193.1 | 159.9 |

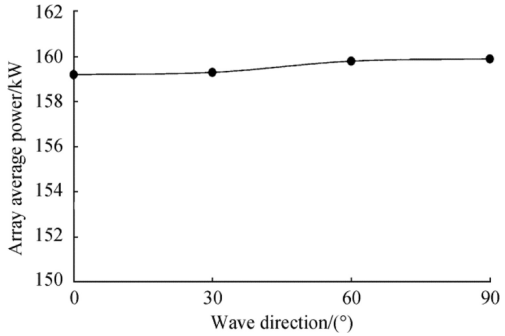


**Fig. 10** Average power generation of six-angle array under different wave directions

1) This paper employs the ANSYS–AQWA time-domain analysis method to achieve the motion simulation and performance analysis of the two-floating-body wave-energy converter array. This method can be an important reference for the analysis of wave-energy arrays in the future.
2) For the simple array of two two-floating-body wave-energy converters, when the space arrangement is reasonable, the power generation of the array is greater than the sum of the power generation of the two wave-energy converters. The effect of $1 + 1 > 2$ can be achieved.
3) In the simple array, the average power generation of the array increases first and then decreases with the increase of arrangement spacing. When the wave-energy converter array is perpendicular to the wave direction, the average generating power is the largest.
4) In a complex array, the average power generation of a six-angle array hardly changes with the wave direction. The average power generation of the six-angle array tends to increase first, then decrease, and then stabilizes as the arrangement spacing increases. An optimal arrangement spacing maximizes the average power generation of the array and does not occupy an excessively large area of the sea.

**Funding Foundation item:** Supported by the National Natural Science Foundation of China under Grant Nos. 5171101175, 11572094, 51809083, and 51579055.

## References

Borgarino B, Babarit A, Ferrant P (2012) Impact of wave interactions effects on energy absorption in large arrays of wave energy converters. Ocean Eng 41:79–88. https://doi.org/10.1016/j.oceaneng.2011.12.025

Budal K (1977) Theory for absorption of wave power by a system of interacting bodies. J Ship Res 21(4):248–253. https://doi.org/10.1016/0022-1694(77)90030-0

Chen X (2013) Time-domain simulation of the motion response of FPSO in waves. Master thesis, Harbin Institute of Technology, Harbin, 32-50

Child BFM (2011) On the configuration of arrays of floating wave energy converters. PhD thesis, University of Edinburgh, Edinburgh

Child BFM, Venugopal V (2010) Optimal configurations of wave energy device arrays. Ocean Eng 37(16):1402–1417. https://doi.org/10.1016/j.oceaneng.2010.06.010

Dai YM (2015) Research on a floating type double floating wave power generation device. Master thesis, South China University of Technology, Guangzhou, 28–65

Eriksson M, Isberg J, Leijon M (2005) Hydrodynamic modelling of a direct drive wave energy converter. Int J Eng Sci 43:1377–1387. https://doi.org/10.1016/j.ijengsci.2005.05.014

Evans DV (1979) Some theoretical aspects of three-dimensional wave-energy absorbers. Proceedings of the First Symposium on Wave Energy Utilization, Chalmers University of Technology, Gothenburg, Sweden, 77–106

Falnes J (1980) Radiation impedance matrix and optimum power absorption for interacting oscillators in surface waves. Appl Ocean Res 2(2):75–80. https://doi.org/10.1016/0141-1187(80)90032-2

Garnaud X, Mei CC (2009) Wave-power extraction by a compact array of buoys. J Fluid Mech 635:389–413

Guan Y (2011) Feasibility study on the development and utilization of wave energy in China. Master thesis, Ocean University of China, Qingdao, 10–30. DOI: https://doi.org/10.7666/d.d169536

Gunn K, Stock-Williams C (2012) Quantifying the global wave power resource. Renew Energy 44(4):296–304. https://doi.org/10.1016/j.renene.2012.01.101

Guo W, Zhou NF, Wang SQ, Zhao QS (2018) Hydrodynamic and capacitated analysis of wave energy devices with nonlinear PTO. Journal of Huazhong University of Science and Technology (Natural Science Edition) 2018(4):57–62. https://doi.org/10.13245/j.hust.180411

Li JY, He HZ (2013) A review of the technical research on wave energy acquisition device. Ocean Development and Management 30(10):67–71. https://doi.org/10.3969/j.issn.1005-9857.2013.10.014

Nazari M, Ghassemi H, Ghiasi M, Sayehbani M (2013) Design of the point absorber wave energy converter for Assaluyeh port. Iranica Journal of Energy & Environment 4(2):130–135. https://doi.org/10.5829/idosi.ijee.2013.04.02.09

Sinha A, Karmakar D, Guedes Soares C (2016) Performance of optimally tuned arrays of heaving point absorbers. Renew Energy 92:517–531. https://doi.org/10.1016/j.renene.2016.02.043

Teng B, Zhao MZ, Jiang SC, Gou Y, Lv L (2010) Calculation and analysis of hydrodynamic coefficient of spar platform heave plate. Ocean Eng 28(3):1–8. https://doi.org/10.3969/j.issn.1005-9865.2010.03.001

Thomas G, Evans DV (1981) Arrays of the three-dimensional wave-energy absorbers. J Fluid Mech 108:67–88. https://doi.org/10.1017/S0022112081001997

Wolgamot HA, Taylor PH, Taylor RE (2012) The interaction factor and directionality in wave energy arrays. Ocean Eng 47:65–73. https://doi.org/10.1016/j.oceaneng.2012.03.017

Xu G, Wang S, Zhu R, Zhang L (2018) Hydrodynamic analysis of variable-pitch vertical axis turbine under yawing motion. Journal of Harbin Engineering University 39(2):304–309. https://doi.org/10.11990/jheu.201608032

Yu YH, Li Y (2013) Reynolds-averaged Navier–Stokes simulation of the heave performance of a two-body floating-point absorber wave energy system. Comput Fluids 73:104–114. https://doi.org/10.1016/j.compfluid.2012.10.007

Zhang XT (2015) Hydrodynamic study of oscillating floating wave energy generator. Master thesis, Shanghai Jiao Tong University, Shanghai, pp 26–45

Zhang L, Dai YS (1992) Time-domain solution to the diffraction problem of objects sailing near the surface. Shipbuilding of China 33(4):1–14

Zhao SM, Liu FY, Zhang JH, Zhang ZH, Bai Y, Zhang R (2008) Basic thinking of China's marine energy development and utilization strategy research. Ocean Technol 27(3):80–83